

**Measurement of Elliptic Flow in p+Au Collisions at $\sqrt{s_{NN}} =$
200 GeV using the PHENIX Detector at RHIC**

by

Theodore Koblesky

B.S., University of Illinois, 2011

A thesis submitted to the
Faculty of the Graduate School of the
University of Colorado in partial fulfillment
of the requirements for the degree of
Doctor of Philosophy
Department of Physics

2017

This thesis entitled:
Measurement of Elliptic Flow in p+Au Collisions at $\sqrt{s_{NN}} = 200$ GeV using the PHENIX
Detector at RHIC
written by Theodore Koblesky
has been approved for the Department of Physics

Professor James Nagle

Prof. Standin

Ms. Standin

Date _____

The final copy of this thesis has been examined by the signatories, and we find that both the content and the form meet acceptable presentation standards of scholarly work in the above mentioned discipline.

Koblesky, Theodore (Ph.D., High Energy Nuclear Physics)

Measurement of Elliptic Flow in p+Au Collisions at $\sqrt{s_{NN}} = 200$ GeV using the PHENIX Detector
at RHIC

Thesis directed by Professor James Nagle

Quark Gluon Plasma (QGP), a hot and dense state of matter in which quarks are not confined inside hadrons, is thought to be the same as the universe approximately one microsecond after the big bang. In Au+Au collisions at $\sqrt{s_{NN}} = 200$ GeV at the Relativistic Heavy Ion Collider (RHIC) and Pb+Pb collisions at $\sqrt{s_{NN}} = 2.76$ TeV at the Large Hadron Collider (LHC), QGP has been discovered to have unique properties, such as its opacity to color charges and the fact it behaves like a near-perfect fluid. Collective behavior in the form of a substantial elliptical azimuthal anisotropy (v_2) in the momentum distribution of final state particles has been observed, indicating a strongly-coupled, hydrodynamically flowing medium. Recently, features of collectivity have been detected in high-multiplicity, small collision systems thought to be too small to produce QGP, such as $^3\text{He}+\text{Au}$ and $d+\text{Au}$ at $\sqrt{s_{NN}} = 200$ GeV, $p + Pb$ at $\sqrt{s_{NN}} = 5$ TeV, and even in $p + p$ at $\sqrt{s} = 13$ TeV events. In order to constrain models seeking to describe this phenomena, collision systems with distinct initial collision geometries were run at RHIC: $^3\text{He}+\text{Au}$ for triangular geometry, $d+\text{Au}$ for elliptical geometry, and $p+\text{Au}$ for circular geometry. This thesis is the completion of that set of three measurements, by measuring v_2 in the $p+\text{Au}$. Comparisons of v_2 in the three collision systems and various theoretical models are made.

Dedication

Acknowledgements

People

Contents

Chapter

1	Experimental Setup	1
1.1	RHIC	1
1.2	PHENIX	3
1.2.1	Forward Rapidity Detectors	4
1.2.1.1	Beam Beam Counter	4
1.2.1.2	Forward Vertex Detector	6
1.2.2	Midrapidity Detectors	7
1.2.2.1	Drift Chamber	7
1.2.2.2	Pad Chambers	8
1.2.2.3	Ring Imaging Cherenkov Detector	9
1.2.2.4	Electromagnetic Calorimeter	9
1.2.3	PHENIX Data Acquisition System	10
1.2.3.1	Triggering	10
1.2.3.2	Event Builder	12
1.2.4	Run 15	13
1.2.4.1	Beam Collision Geometry	14
1.2.5	Centrality Determination	15

Tables

Table

1.1	An example Run15 p+Au 200 GeV relevant trigger configuration and parameters.	
	A trigger's scale down number reduces its rate by $1/(1+\text{scale down})$.	11
1.2	Some relevant RHIC parameters from Run 15.	13

Figures

Figure

1.1	A helicopter's view of the accelerator chain in BNL starting at the Tandems (in gold) and ending at the RHIC ring (in blue). STAR and PHENIX can be seen at two of the interaction regions. The ring is 2.38 miles in circumference.	2
1.2	The top is a cross section diagram of the PHENIX detector from the incoming beam's perspective. The bottom is a cross section diagram of the PHENIX detector from the top down. The central arm detectors are not present in the bottom diagram. add ref	5
1.3	Photographs of the BBC detector. The left is of a single detector element consisting of a quartz Cherenkov and a PMT. The right is of one of the BBC arms, consisting of 64 detector elements. add ref	6
1.4	A photograph of half of the FVTX. The FVTX are the half disks on either end of the picture (left) and a schematic of the FVTX at a slightly different angle (right). The FVTX is only 20 cm in the z direction from the PHENIX coordinate system origin (the center of the picture). add ref	7
1.5	A diagram of the DC titanium frame which encloses the detector.	8
1.6	A diagram of the X, U, and V wires in the DC.	9
1.7	Diagram of a granule. Granules are the building blocks of the PHENIX DAQ. Each detector subsystem has at least one granule.	12
1.8	Diagram of the event builder.	13

1.9 The distribution of BBC charges in p+Au 200 GeV events for different triggers. The black curve is the distribution of charges for the minbias trigger. The blue and red curves are the distributions of charges for the high multiplicity trigger. The red curve being scaled by a factor of 1/40 to show agreement with the black curve. The definition of the top 5% more central events are BBC south charges ≥ 48.0 . The plot shows the large enhancement of the number of 0-5% centrality events that are gained using the high multiplicity trigger compared to the number of 0-5% centrality from the minbias trigger alone.	14
1.10 A vector diagram illustrating the yellow and blue beam angle confirmation relative to the PHENIX coordinate system.	15
1.11 The distribution of BBC calculated z-vertex positions for events in p+Au 200 GeV. There are more events between -10 and 10 cm because of the BBC narrow trigger. .	16
1.12 The distribution of the length of physics runs.	16
1.13 Integrated luminosity from the p+Au dataset.	17
1.14 A Monte Carlo Glauber d+Au event display. Each circle is a nucleon. The red nucleons are from the projectile (deuteron) and the green nucleons are participants from the target (gold). Glauber counts even a near miss as a full collision.	17
1.15 Real data for BBC Charge South (Au-going direction) shown as open circles and Glauber Monte Carlo + NBD. The colors correspond to the various percentiles relative to the total inelastic p+Au cross section, the most central 0-5% in solid red. The blue and red curves correspond to the Level-1 trigger efficiency in all inelastic collisions and inelastic collisions producing a particle at midrapidity, respectively. The best fit NBD parameters are $\mu = 3.14$, $k = 0.47$, and the trigger firing on 84 +/- 3% of the total inelastic cross section [$\sigma = 1.76$ barns].	18

Chapter 1

Experimental Setup

1.1 RHIC

The Relativistic Heavy Ion Collider (RHIC) is a superconducting charged hadron collider located at Brookhaven National Labs (BNL) in Upton, NY, United States. RHIC is capable of accelerating heavy ions such as Au (gold) or Cu (copper) nuclei to energies of ~ 100 GeV per nucleon. RHIC is also capable of accelerating lighter ions such as protons, deuteron, and helium to ~ 100 GeV per nucleon and ~ 250 GeV per proton in the case of protons. The machine has been demonstrated the ability to reliably create the so called QGP (Quark Gluon Plasma) matter.

There are two major detector experiments currently operating in interaction regions around the RHIC ring: PHENIX (Pioneering High Energy Nuclear Interaction eXperiment) and STAR (Solenoidal Tracker at RHIC). Figure 1.1 shows the locations of the experiments and the accelerator chain. A typical operation schedule for RHIC is to run the accelerator for five and a half months every year in what is called a "Run". There have been 16 Runs so far but the relevant run for this thesis was the 15th run taken in 2015 which ran proton colliding with gold ions ($p+Au$) $\sqrt{s_{NN}} = 200$ GeV for part of its running. Specific details about this dataset are found in section 1.2.4.

RHIC is at the end of a chain of smaller accelerators that are used to "feed" the ions into RHIC, where they are accelerated (or decelerated in some circumstances) to the desired collision energy. For heavy ions such as Au, the process is listed in detail below [44].

- (1) A pulsed sputter Au ion source generates negative ions in the Tandem Van De Graaff.

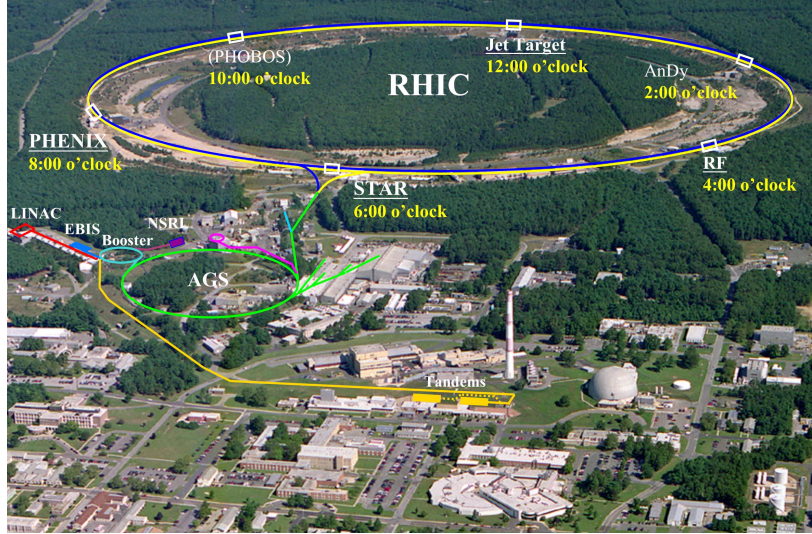


Figure 1.1: A helicopter's view of the accelerator chain in BNL starting at the Tandems (in gold) and ending at the RHIC ring (in blue). STAR and PHENIX can be seen at two of the interaction regions. The ring is 2.38 miles in circumference.

- (2) The ions are passed through an electron stripping foil to achieve a positive 12 charge and accelerated to ~ 1 MeV per nucleon.
- (3) The ions pass through bending magnets and another foil to further strip electrons and filter charge, yielding to a positive 32 charge state.
- (4) The ions are sent to the Booster Synchrotron which accelerates them to 95 MeV per nucleon and leaves them at a positive 77 charge.
- (5) The ions enter the Alternating Gradient Synchrotron (AGS) in bunches of 24 ions. The ions are debunched and rebunched into four bunches and then accelerated to 10.8 GeV per nucleon.
- (6) The bunches then exit the AGS one at a time, where their Au ions are stripped of their two remaining electrons, yielding a final charge state of positive 79. Finally, the bunches are transferred to their respective buckets in RHIC .

For protons, the process instead begins at the the Linear Accelerator (LINAC) facility. The

protons are then sent through the chain of accelerators in a similar way to the heavy ions until reaching RHIC in either a polarized or unpolarized state.

Once the ions have reached RHIC, they will enter one of two independent rings, blue or yellow, each circulating in an opposite direction. The ions in the rings are deflected and focused by 1,740 superconducting magnets using niobium-titanium conductors. Once the ions are focused and accelerated to the desired parameters around the RHIC, the ions are deflected into the six interactions regions where the blue and yellow rings intersect to produce collisions. It is at these interaction regions where the major experiments have set up their detectors, with STAR at the 6 o'clock position and PHENIX at the 8 o'clock position.

The period of time that collisions continue is known as a fill, and the average length of a fill is eight hours. As the fill wears on, the collision rate substantially decreases as the density of ions in the machine decreases. Once the collision rate has been reduced sufficiently, it is more cost efficient to start the fill over at a higher collision rate.

1.2 PHENIX

PHENIX, the Pioneering High Energy Nuclear Interaction eXperiment, came online in 2000 along with RHIC and is located at the 8 o'clock interaction region along the RHIC ring. PHENIX is one of the two major RHIC experiments along with STAR, the Solenoidal Tracker At RHIC. The PHENIX detector philosophy differs from STAR in that PHENIX has a small acceptance but very good PID (particle identification) capabilities.

PHENIX's detectors throughout the years include (in no particular order) the Drift Chamber (DC), the Pad Chambers (PC), the Ring Imaging Cherenkov (RICH) Detector, the Hadron Blind Detector (HBD), the Time Expansion Chamber (TEC), the Time of Flight (TOF), the Electromagnetic Calorimeter (EMCAL), the Muon Tracker (MuTr), the Muon Identifier (MuID), the Muon Piston Calorimeter (MPC), the Muon Piston Calorimeter Extension (MPC-EX), the Beam-Beam Counter (BBC), the Zero Degree Calorimeter (ZDC), the Forward Calorimeter (FCAL), the Multiplicity and Vertex Detector (MVD), the Reaction Plane Detector (RPD), the Resistive Plate

Chambers (RPC), the Silicon Vertex Detector (VTX), and the Forward Silicon Vertex Detector (FVTX). Figure 1.2 depicts the approximate size and position of each of the detectors which are installed in PHENIX as of 2015.

For this thesis, the relevant detectors installed in 2015 are the DC, PC, RICH, BBC, and FVTX. The DC, PC, and RICH are located in the mid-rapidity region relative to collisions (Central Arms) and the BBC and FVTX are located in the forward (and backward) rapidity region relative to collisions (Forward Arms) [18].

PHENIX makes use of the three powerful magnets in order to bend charged the particles' trajectories: the Central Magnet (CM), the North Muon Magnet (MMN), and the South Muon Magnet (MMS). For this thesis, the relevant magnet is the CM.

PHENIX makes use of a state of the art Data Acquisition System (DAQ) which is capable of writing 400 MB/s of information to disk. More details about the PHENIX DAQ are found in section ??.

1.2.1 Forward Rapidity Detectors

1.2.1.1 Beam Beam Counter

The BBC is a forward detector used to determine the event start time, vertex, centrality, and event plane. The BBC is composed of two mirror image arrays, a South and a North Arm, that surround the beam pipe 144 cm on opposite sides of the nominal collision point just behind the Central Magnet, covering $3.0 < |\eta| < 3.9$ and 2π radians in azimuth. Each BBC arm is made of 64 elements each composed of a 3-cm length quartz Cherenkov radiator connected to a 2.5 cm diameter Hamamatsu R6178 mesh dynode PMT (photomultiplier tube), as shown in Fig 1.3. The outer and inner diameters of the BBC are 30 cm and 10 cm, respectively.

The BBC is used to mark the event start time for the entire PHENIX detector by averaging the emitted particles arrival time at each BBC arm. The timing difference between each arm

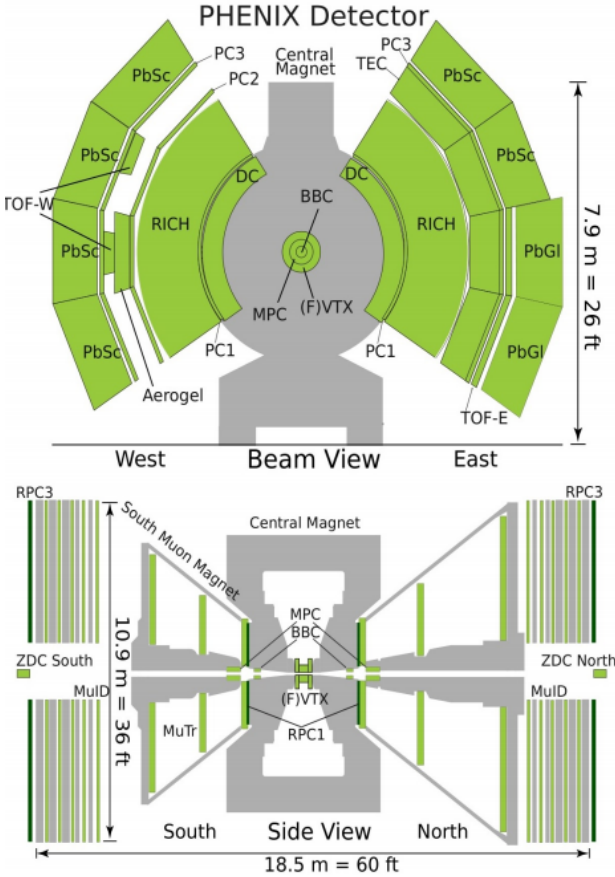


Figure 1.2: The top is a cross section diagram of the PHENIX detector from the incoming beam's perspective. The bottom is a cross section diagram of the PHENIX detector from the top down. The central arm detectors are not present in the bottom diagram.**add ref**

provides an estimate of the collision's z-vertex by

$$z = c \frac{T_S - T_N}{2}, \quad (1.1)$$

where T_S, T_N are the particle's average arrival times for each arm and c is the speed of light. For p+Au at $\sqrt{s_{NN}} = 200$ GeV collisions, the BBC has a timing resolution of ps ~ 40 ps and a z-vertex resolution of $\sim 1.0\text{-}2.0$ cm, depending on the event charged particle multiplicity. This rough estimate of the vertex is used during triggering. Specific details about triggers are in section 1.2.3.

The BBC also provides the centrality classification, as described in Chapter 2 Section ??, of a collision event in PHENIX. Details of how BBC data is used to compute the centrality are given

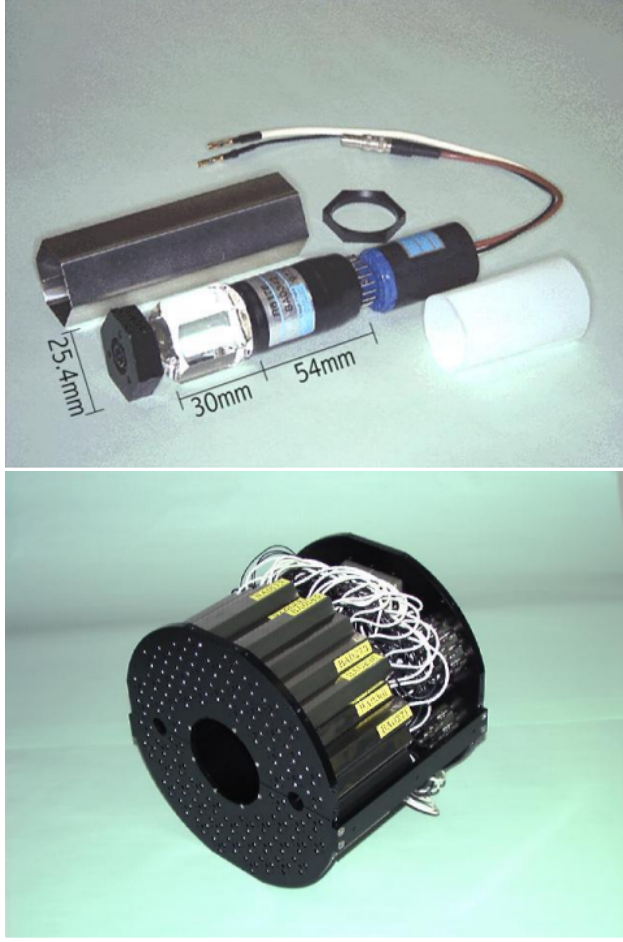


Figure 1.3: Photographs of the BBC detector. The left is of a single detector element consisting of a quartz Cherenkov and a PMT. The right is of one of the BBC arms, consisting of 64 detector elements.**add ref**

later in this Chapter in section 1.2.5.

1.2.1.2 Forward Vertex Detector

The FVTX is a PHENIX detector upgrade which became operational for physics data taking in 2012. The FVTX uses charged particle tracking, collision vertex determination, and event plane determination [17]. The FVTX consists of two identical endcaps covering a combined pseudorapidity range of $1 < |\eta| < 3$ and full azimuth coverage. Each endcap has four stations of silicon mini-strip sensors with a pitch of $75 \mu\text{m}$ arranged in the radial direction around the beam pipe.

The basic unit of construction is a wedge that has a silicon strip sensor and read-out chips. There are four FVTX layers in each endcap. Figure 1.4 is a

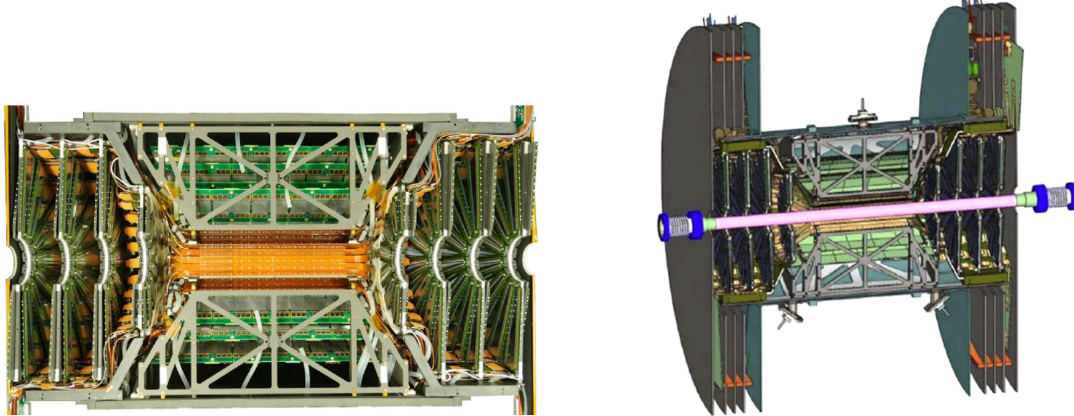


Figure 1.4: A photograph of half of the FVTX. The FVTX are the half disks on either end of the picture (left) and a schematic of the FVTX at a slightly different angle (right). The FVTX is only 20 cm in the z direction from the PHENIX coordinate system origin (the center of the picture).[add ref](#)

1.2.2 Midrapidity Detectors

1.2.2.1 Drift Chamber

The DC consists of two gas multi-wire chambers, one located in each arm. The DC is used to measure particle trajectories in the $r\phi$ plane. The DC is the innermost subsystem in the central arms, located 2 m from the z-axis, placing it in a residual magnetic field of 0.6 kiloGauss from the CM. Apart from the VTX, the DC is the first detector encountered by a particle in mid-rapidity.

As a charged particle passes through the DC volume, the gases are ionized to create free electrons. These electrons cause a chain reaction of ionizations which are measured by an anode wire. The DC is designed in such a way that the drift velocities of the electrons are predictable enough to relate time and position together.

Each identical DC arm is cylindrical in design and covers 2.5 m along the beam direction and is 0.4 m thick as seen Fig 1.5. A gas mixture of 50% Argon and 50% Ethane is used in each arm of

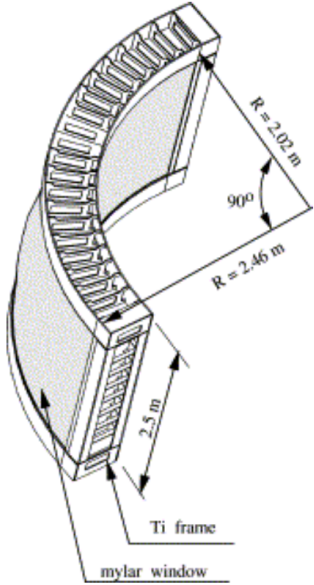


Figure 1.5: A diagram of the DC titanium frame which encloses the detector.

the DC. Each arm is divided into 20 equal sectors covering 4.5 degrees in ϕ . Each sector contains six types of wire modules stacked radially and labeled X1, U1, V1, X2, U2, V2, respectively from the inside out. The X wires run parallel to the beam to perform precise four ϕ measurements while the U and V wires are set at small angles of about six degrees relative to the X wires to provide information about the z position of the track. A diagram of the wire layout in each sector is shown in Figure 1.6. In total, the DC consists of 6500 anode wires leading to 13,000 readout channels, with a measured single wire resolution of 165 m and a spatial resolution of 2 mm.

1.2.2.2 Pad Chambers

The PCs are multi-wire proportional chambers which consist of three separate layers of detectors measuring precise hit positions and making up the bulk of the PHENIX tracking system. The innermost layer, PC1, is located in both the East and West arms immediately outside the DC, providing a measurement of the z position at the back plane of the DC. The second layer, PC2, is located behind the RICH in the West arm only. The outer layer, PC3, is in both arms and provides

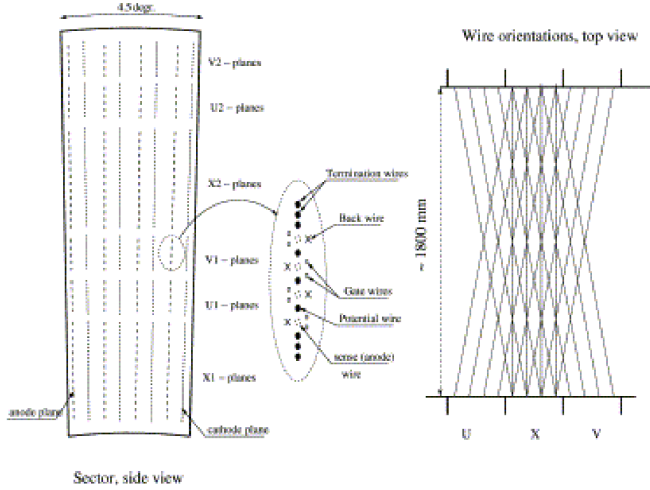


Figure 1.6: A diagram of the X, U, and V wires in the DC.

a second point on the straight line trajectories of the tracks through the detector, outside of the magnetic field.

1.2.2.3 Ring Imaging Cherenkov Detector

The RICH detector is located immediately behind the PC1 and provides the primary electron identification for PHENIX. The RICH consists of two identical detectors located in each arm and provides e over π discrimination below the pion Cherenkov threshold of 4.65 GeVc in the CO₂ gas used in the detectors.

1.2.2.4 Electromagnetic Calorimeter

The EMCAL is the outermost subsystem in the central arms and is designed primarily to measure the energies and positions of photons and electrons. It also plays a key role in the identification of as well as providing triggering for rare events. Two different EMCAL designs were utilized with 6 sectors based on a lead-scintillator design and 2 sectors based on a lead-glass design. The two different designs were chosen deliberately as each provides advantages and disadvantages, for instance the lead glass has a better energy resolution, while the lead scintillator has better linearity

and timing.

1.2.3 PHENIX Data Acquisition System

PHENIX makes use of a fast DAQ to manage the transfer and collation of hundreds of kB of event data from over two dozen independent detector subsystems at a rate of over 6 kHz. This amounts to writing to disk hundreds of MB/s, something which the PHENIX DAQ consistently achieves for months of around the clock use.

The collection of a Granule Timing Module (GTM), Front End Modules (FEM), and a Data Collection Modules (DCM) is known as a granule and is the minimal combination of DAQ hardware sufficient for data production as shown in Fig 1.2.3.1. Each detector subsystem's output data is managed by a granule. Pipelined Field ProGrammable Arrays (FPGA) with carefully controlled dead time are used to calculate the trigger decisions. The FPGAs are fed information from the experiment. Once the FPGAs compute the trigger decision, the trigger signals are monitored by the GTM. If trigger decision is positive, the GTMs instruct the FEMs to release their data from their buffers and send them to their graunules' DCM. If the decision is negative, otherwise the FEMs are instructed to dump the data. Once the DCM is instructed to send its data downstream, it is sent to the event builder which will be discussed in an upcoming section.

1.2.3.1 Triggering

PHENIX has the capability of running 128 independent triggers, in practice only 32 are used. Each of the triggers have a scale down number to control the relative bandwidth each trigger receives. To understand the PHENIX triggers, it is useful to learn about the beam clock.

The PHENIX trigger is tied to the clock of the blue beam, one of the two counter circulating rings of which RHIC is comprised. The clock rate is fixed at 9.38 MHz and is tied to the rate at which RHIC overlaps bunches of ions in the interaction regions. Every time a bunch of ions from the blue ring overlap with a bunch of ions from the yellow ring, there is a blue clock trigger. This clock is stable by necessity of the precision required to run a complex accelerator like RHIC. This

blue clock trigger is the backbone of PHENIX triggering for there can be no ion collision event if there is no overlap of bunches. Consequently, almost every PHENIX trigger is AND'd with the clock trigger.

The trigger which is given the largest bandwidth is the minimum bias (minbias) trigger. As the name suggests, the trigger seeks to mark the detection of an ion collision while reducing the any bias to the type of the collision to a minimum. To achieve this, data from the BBC and ZDC are used, although the ZDC is less relevant than the BBC for defining the trigger. Although what constitutes a minbias observation varies with collision species, the BBC minbias trigger is generally defined as >0 PMTs in each arm above threshold. Not only is this condition a good indication that a ion collision occurred, it is also the minimum information necessary to calculate the collision vertex position using the BBC. The vertex information is important because it is used to select for collisions which occur in the narrow range of acceptance of current PHENIX detector configuration. This range is $-10 \text{ cm} < z < 10 \text{ cm}$ where z is defined in the PHENIX coordinate system in fig (TBA). For completeness, PHENIX takes BBC minbias triggers with z vertex cuts of 30 cm and with no vertex cut. The collection of all these triggers is what is considered to be the PHENIX minbias trigger.

In Run 15, a unique high multiplicity trigger was implemented to enhance event statistics for events producing the most amount of particles. This trigger consisted of requiring at least 35 out of 64 PMTs in the south arm of the BBC. More details about this trigger are located in section 1.2.4.

Table 1.1: An example Run15 p+Au 200 GeV relevant trigger configuration and parameters. A trigger's scale down number reduces its rate by $1/(1+\text{scale down})$.

<i>Trigger Name</i>	<i>Scale down</i>	<i>Trigger rate</i>	<i>Vertex cut</i>	<i>Part of minbias</i>
<i>Clock</i>	196077	45Hz	N/A	<i>no</i>
<i>BBC(> 0 PMTs)</i>	100	695Hz	10cm	<i>yes</i>
<i>BBC(> 0 PMTs)</i>	2083	88Hz	30cm	<i>yes</i>
<i>BBC(> 0 PMTs)</i>	3959	94Hz	<i>no cut</i>	<i>yes</i>
<i>BBC(> 35 PMTs)</i>	1	1640Hz	10cm	<i>no</i>

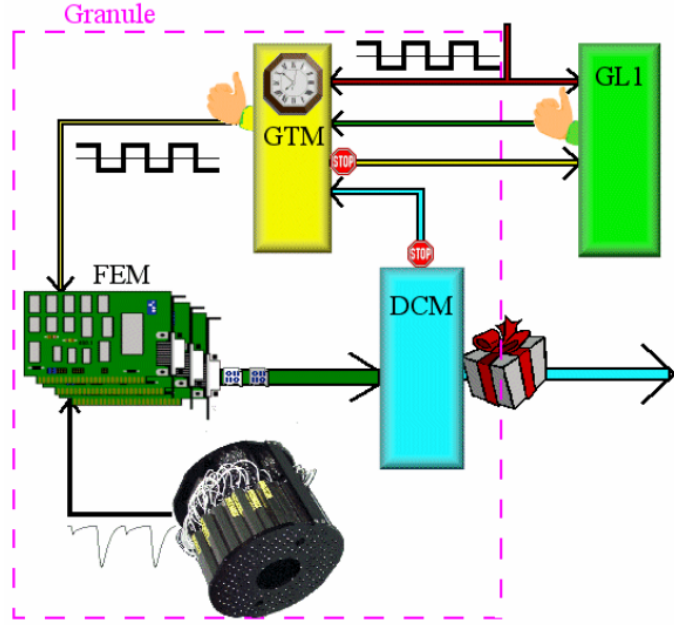


Figure 1.7: Diagram of a granule. Granules are the building blocks of the PHENIX DAQ. Each detector subsystem has at least one granule.

1.2.3.2 Event Builder

Following the PHENIX DAQ downstream, after a positive trigger decision has been sent to each of the granules, the granules' data packets are sent to the event builder. It is the event builder's job to associate each granule's data packet from the same collision event into one bundle of data known as an event. The event builder consists of Sub Event Buffers (SEB), Assembly Trigger Processors (ATP), an Event Builder Controller (EBC), and a Gigabit Ethernet Switch as the communication management. Fig 1.8 provides a diagram of how these components are connected.

Granules send the data packets to the specific SEB assigned to that granule. The EBC receives global trigger information and assigns each ATP a specific collision event. The ATP then requests the data from all of the SEBs for the specific event assigned to it by the EBC. Once the ATP is successful, it writes the assembled event to disk and the EBC instructs the SEBs to flush the buffer for that event.

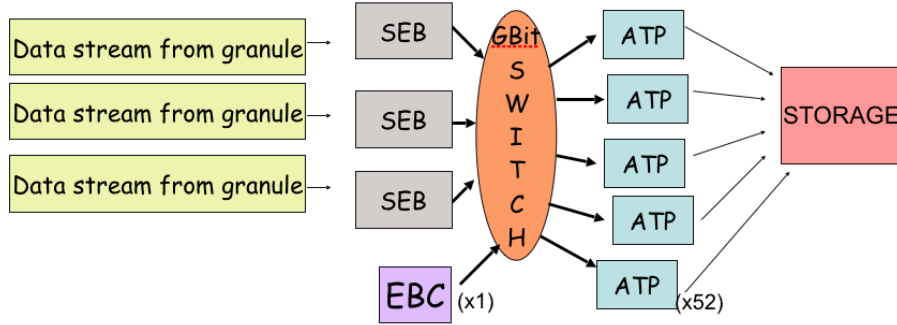


Figure 1.8: Diagram of the event builder.

1.2.4 Run 15

Run 15 is the RHIC running period in the year 2015 which marks fifteen consecutive years of RHIC running since the year 2000. Run 15 began in January 2015 and ended in June of 2015. There were approximately eleven weeks of research viable, polarized p+p collisions at $\sqrt{s} = 200$ GeV, approximately 5 weeks of research viable polarized p+Au collisions at $\sqrt{s} = 200$ GeV, and approximately one week of research viable p+Al collisions $\sqrt{s} = 200$ GeV. Of interest to this thesis are the p+p and p+Au datasets.

Table 1.2: Some relevant RHIC parameters from Run 15.

Collision Species	p+p	p+Au	units
Total Particle Energy	100.2	$103.9 + 100.0$	GeV/nucleon
Ions per Bunch	225	$225 + 1.6$	number $\times 10^9$
Number of Bunches	111	111	number
Luminosity Average Per Fill	63×10^{30}	45×10^{28}	$cm^{-2}s^{-1}$
Total Delivered Luminosity	382	1.27	pb^{-1}
Average Fill Lifetime	8	7	hours

In addition to providing the min-bias trigger for Run 15, the BBC was used to implement a high-multiplicity trigger in order to enhance the amount of the top 5% highest multiplicity events. The high-multiplicity trigger requires 35 of the 64 BBC south arm PMTs to be above threshold in a given event to be satisfied. The relevant BBC arm for p+Au is the south arm since that is the

Au-going direction so the multiplicity is much higher in the south arm. The enhancement can be seen in Figure 1.9.

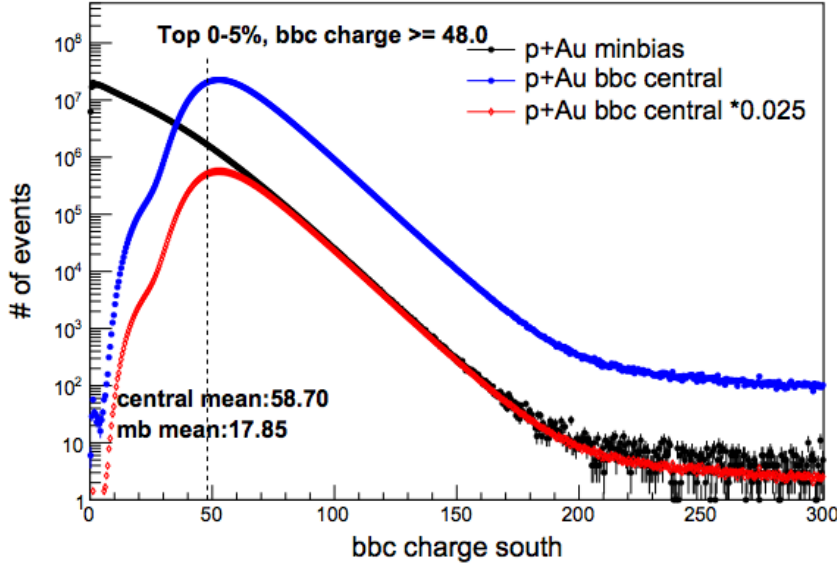


Figure 1.9: The distribution of BBC charges in p+Au 200 GeV events for different triggers. The black curve is the distribution of charges for the minbias trigger. The blue and red curves are the distributions of charges for the high multiplicity trigger. The red curve being scaled by a factor of 1/40 to show agreement with the black curve. The definition of the top 5% more central events are BBC south charges ≥ 48.0 . The plot shows the large enhancement of the number of 0-5% centrality events that are gained using the high multiplicity trigger compared to the number of 0-5% centrality from the minbias trigger alone.

1.2.4.1 Beam Collision Geometry

For Run 15 p+Au 200 GeV running, RHIC's blue and yellow beams were not in perfect accordance to the PHENIX coordinate system. This was manifested in two separate ways. First of all, the collision vertex is significantly offset from the z-axis to which all of the PHENIX detectors are aligned. This is a typical situation in PHENIX datasets but it must be addressed. The other effect, and the more significant of the two, comes from the fact that the beams are colliding at an angle of 3.6 milli-Radians in the x-z plane as illustrated in Fig 1.10. This is a result of configuring RHIC magnets for the specific charge to mass ratios of the p+Au collision species. The collision

vertex in x and y is known as the beam center. The beam center varies over the course of data taking but its values on average are $(x, y) = (0.206, 0.065)(cm)$. The distribution of z-vertices from collision events can be seen in Fig 1.11. Due to the fact that the beams are colliding at an angle in the x - z plane, the x -component of the beam center will have a z-vertex dependence with a slope of -0.0036 cm of x per 1 cm of z . Apart from how the beam angle effects the beam center values, it also violates the expectation of a uniform ϕ distribution of particles with respect to PHENIX detectors. PHENIX detectors are designed and aligned with respect to the PHENIX coordinate system with the expectation of geometric symmetry. A significant beam collision angle with respect to PHENIX detectors would be equivalent to PHENIX detectors being tilted which would violate geometric symmetry. The physics analysis described in this thesis is sensitive to these beam geometry effects. A discussion on how to account for these effects will be in chapter 4.

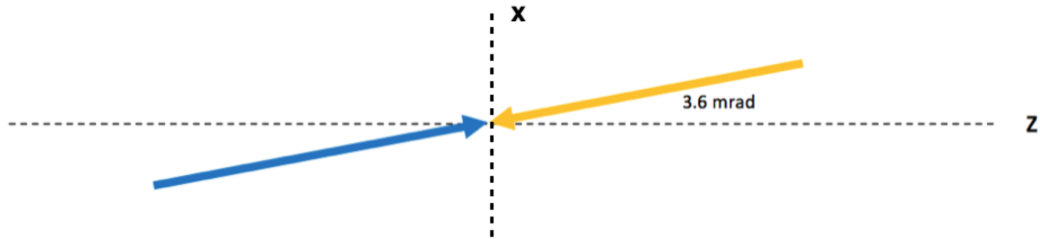


Figure 1.10: A vector diagram illustrating the yellow and blue beam angle confirmation relative to the PHENIX coordinate system.

1.2.5 Centrality Determination

The centrality determination is done by adding up all BBC South (Au-going direction) PMT charges for every event and then splitting up that distribution into equivalent centrality bins. This procedure can be used to associate a centrality bin with number of binary collisions from Monte Carlo Glauber + Negative Binomial Distribution (NBD). An example of such an event for d+Au is seen in Fig 1.14.

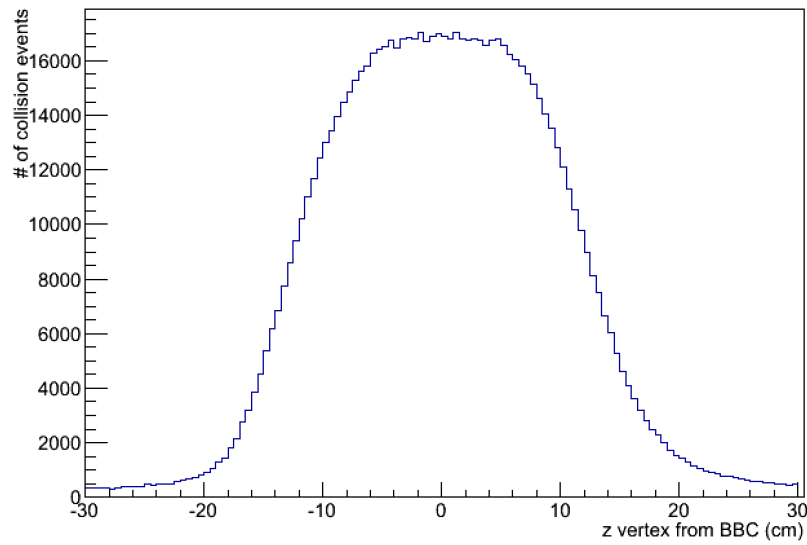


Figure 1.11: The distribution of BBC calculated z-vertex positions for events in p+Au 200 GeV. There are more events between -10 and 10 cm because of the BBC narrow trigger.

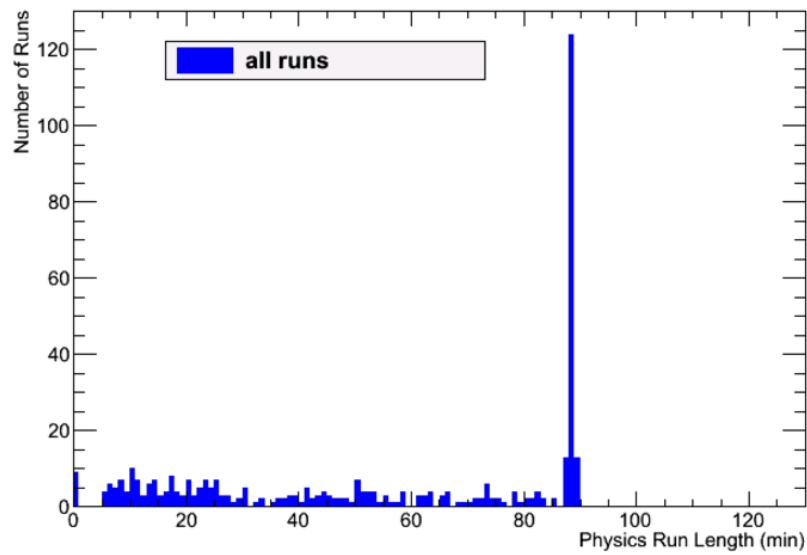


Figure 1.12: The distribution of the length of physics runs.

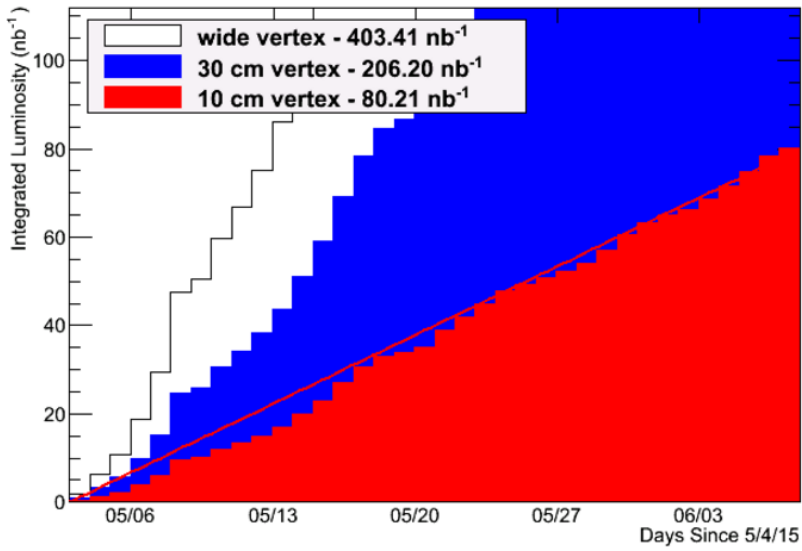


Figure 1.13: Integrated luminosity from the p+Au dataset.

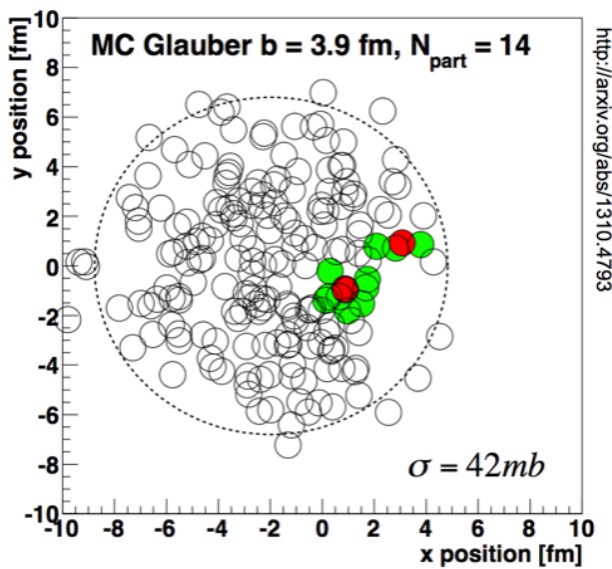


Figure 1.14: A Monte Carlo Glauber d+Au event display. Each circle is a nucleon. The red nucleons are from the projectile (deuteron) and the green nucleons are participants from the target (gold). Glauber counts even a near miss as a full collision.

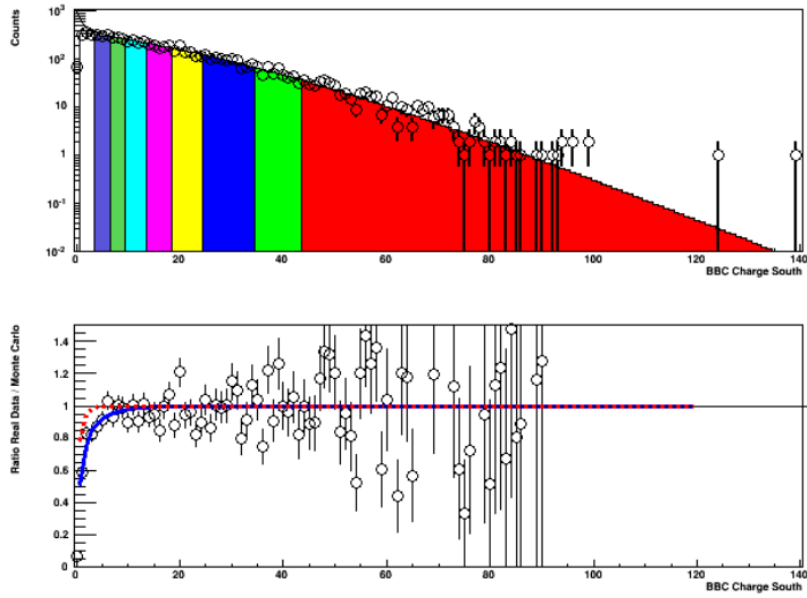


Figure 1.15: Real data for BBC Charge South (Au-going direction) shown as open circles and Glauber Monte Carlo + NBD. The colors correspond to the various percentiles relative to the total inelastic p+Au cross section, the most central 0-5% in solid red. The blue and red curves correspond to the Level-1 trigger efficiency in all inelastic collisions and inelastic collisions producing a particle at midrapidity, respectively. The best fit NBD parameters are $\mu = 3.14$, $k = 0.47$, and the trigger firing on $84 \pm 3\%$ of the total inelastic cross section [sigma = 1.76 barns].

Bibliography

- [1]
- [2] Event reconstruction in the {PHENIX} central arm spectrometers. *Nucl.Instrum.Meth*, A482:491–512, 2002.
- [3] Rhic operations with asymmetric collisions in 2015. 2015.
- [4] K. Aamodt and et al. Harmonic decomposition of two particle angular correlations in pbpb collisions at. *Physics Letters B*, 708(35):249 – 264, 2012.
- [5] F. D. et al Aaron. Inclusive deep inelastic scattering at high q₂ with longitudinally polarised lepton beams at hera. *Journal of High Energy Physics*, 2012(9):61, 2012.
- [6] A. et al Adare. Measurements of elliptic and triangular flow in high-multiplicity ³He + Au collisions at $\sqrt{s_{NN}} = 200$ GeV. *Phys. Rev. Lett.*, 115:142301, Sep 2015.
- [7] S. S. et al Adler. Absence of suppression in particle production at large transverse momentum in $\sqrt{s_{NN}} = 200$ GeV d + Au collisions. *Phys. Rev. Lett.*, 91:072303, Aug 2003.
- [8] Yasuyuki Akiba et al. The Hot QCD White Paper: Exploring the Phases of QCD at RHIC and the LHC. 2015.
- [9] J. et al Beringer. Review of particle physics. *Phys. Rev. D*, 86:010001, Jul 2012.
- [10] Siegfried Bethke. The 2009 world average of α . *The European Physical Journal C*, 64(4):689–703, 2009.
- [11] Rajeev S. Bhalerao. Relativistic heavy-ion collisions. In *Proceedings, 1st Asia-Europe-Pacific School of High-Energy Physics (AEPSHEP)*: Fukuoka, Japan, October pages 219–239, 2014.
- [12] Adam Bzdak and Guo-Liang Ma. Elliptic and triangular flow in p-pb and peripheral pb-pb collisions from parton scatterings. *Phys. Rev. Lett.*, 113:252301, Dec 2014.
- [13] M. Cheng, S. Ejiri, P. Hegde, F. Karsch, O. Kaczmarek, E. Laermann, R. D. Mawhinney, C. Miao, S. Mukherjee, P. Petreczky, C. Schmidt, and W. Soeldner. Equation of state for physical quark masses. *Phys. Rev. D*, 81:054504, Mar 2010.
- [14] Fred Cooper and Graham Frye. Single-particle distribution in the hydrodynamic and statistical thermodynamic models of multiparticle production. *Phys. Rev. D*, 10:186–189, Jul 1974.

- [15] Kevin Dusling and Raju Venugopalan. Azimuthal collimation of long range rapidity correlations by strong color fields in high multiplicity hadron-hadron collisions. *Phys. Rev. Lett.*, 108:262001, Jun 2012.
- [16] S. Eremin and S. Voloshin. Nucleon participants or quark participants? *Phys. Rev. C*, 67:064905, Jun 2003.
- [17] C. Aidala et al. The {PHENIX} forward silicon vertex detector. *Nuclear Instruments and Methods in Physics Research Section A: Accelerators, Spectrometers, Detectors and Associated Equipment*, 755:44 – 61, 2014.
- [18] K. Adcox et al. {PHENIX} detector overview. *Nuclear Instruments and Methods in Physics Research Section A: Accelerators, Spectrometers, Detectors and Associated Equipment*, 499(2?3):469 – 479, 2003. The Relativistic Heavy Ion Collider Project: {RHIC} and its Detectors.
- [19] A Fedotov. Progress of high-energy electron cooling for rhic.
- [20] Enrico Fermi. High energy nuclear events. *Progress of Theoretical Physics*, 5(4):570–583, 1950.
- [21] A. D. Frawley. Cold Nuclear Matter Effects and Heavy Quark Production in PHENIX. *Nucl. Phys.*, A910-911:123–130, 2013.
- [22] Charles Gale, Sangyong Jeon, Björn Schenke, Prithwish Tribedy, and Raju Venugopalan. Event-by-event anisotropic flow in heavy-ion collisions from combined yang-mills and viscous fluid dynamics. *Phys. Rev. Lett.*, 110:012302, Jan 2013.
- [23] M. Habich, J. L. Nagle, and P. Romatschke. Particle spectra and hbt radii for simulated central nuclear collisions of .
- [24] M. Habich, J. L. Nagle, and P. Romatschke. Particle spectra and hbt radii for simulated central nuclear collisions of c+c, al+al, cu+cu, au+au, and pb+pb from $\sqrt{s}=62.4\text{--}2760$ gev. *The European Physical Journal C*, 75(1):15, 2015.
- [25] Ulrich W. Heinz. Towards the Little Bang Standard Model. *J. Phys. Conf. Ser.*, 455:012044, 2013.
- [26] Tetsufumi Hirano, Ulrich Heinz, Dmitri Kharzeev, Roy Lacey, and Yasushi Nara. Mass ordering of differential elliptic flow and its violation for ϕ mesons. *Phys. Rev. C*, 77:044909, Apr 2008.
- [27] V. Khachatryan and et al. Evidence for collectivity in pp collisions at the {LHC}. *Physics Letters B*, 765:193 – 220, 2017.
- [28] V. Khachatryan and et al. Observation of long-range, near-side angular correlations in proton-proton collisions at the lhc. *Journal of High Energy Physics*, 2010(9):91, 2010.
- [29] Peter F. Kolb and Ulrich W. Heinz. Hydrodynamic description of ultrarelativistic heavy ion collisions. 2003.
- [30] Zi-Wei Lin, Che Ming Ko, Bao-An Li, Bin Zhang, and Subrata Pal. Multiphase transport model for relativistic heavy ion collisions. *Phys. Rev. C*, 72:064901, Dec 2005.

- [31] Matthew Luzum and Paul Romatschke. Conformal relativistic viscous hydrodynamics: Applications to rhic results at $\sqrt{s_{NN}} = 200$ gev. *Phys. Rev. C*, 78:034915, Sep 2008.
- [32] Guo-Liang Ma and Zi-Wei Lin. Predictions for $\sqrt{s_{NN}} = 5.02$ tev pb + pb collisions from a multiphase transport model. *Phys. Rev. C*, 93:054911, May 2016.
- [33] Stephen J. Sanders Michael L. Miller, Klaus Reygers and Peter Steinberg. Glauber modeling in high-energy nuclear collisions. *Annual Review of Nuclear and Particle Science*, 57:205–243, 2007.
- [34] J. Scott Moreland, Jonah E. Bernhard, and Steffen A. Bass. Alternative ansatz to wounded nucleon and binary collision scaling in high-energy nuclear collisions. *Phys. Rev. C*, 92:011901, Jul 2015.
- [35] J. L. Nagle, A. Adare, S. Beckman, T. Koblesky, J. Orjuela Koop, D. McGlinchey, P. Romatschke, J. Carlson, J. E. Lynn, and M. McCumber. Exploiting intrinsic triangular geometry in relativistic ${}^3\text{He} + \text{Au}$ collisions to disentangle medium properties. *Phys. Rev. Lett.*, 113:112301, Sep 2014.
- [36] J. D. Orjuela Koop, A. Adare, D. McGlinchey, and J. L. Nagle. Azimuthal anisotropy relative to the participant plane from a multiphase transport model in central $p + \text{Au}$, $d + \text{Au}$, and ${}^3\text{He} + \text{Au}$ collisions at $\sqrt{s_{NN}} = 200$ gev. *Phys. Rev. C*, 92:054903, Nov 2015.
- [37] A. Ortiz Velasquez, P. Christiansen, E. Cuautle Flores, I. A. Maldonado Cervantes, and G. Paić. Color reconnection and flowlike patterns in pp collisions. *Phys. Rev. Lett.*, 111:042001, Jul 2013.
- [38] A. M. Poskanzer and S. A. Voloshin. Methods for analyzing anisotropic flow in relativistic nuclear collisions. *Phys. Rev. C*, 58:1671–1678, Sep 1998.
- [39] Guang-You Qin. Anisotropic Flow and Jet Quenching in Relativistic Nuclear Collisions. *Int. J. Mod. Phys., E24(02):1530001*, 2015.
- [40] Johann Rafelski. Connecting qgp-heavy ion physics to the early universe. *Nuclear Physics B - Proceedings Supplements*, 243:155 – 162, 2013.
- [41] Johann Rafelski and Jeremiah Birrell. Traveling through the universe: Back in time to the quark-gluon plasma era. *Journal of Physics: Conference Series*, 509(1):012014, 2014.
- [42] Eric Michael Richardson. Elliptic flow at forward rapidity in $\sqrt{s_{NN}} = 200$ GeV Au+Au collisions. PhD thesis, Maryland U., 2012.
- [43] P. Romatschke. Light-heavy-ion collisions: a window into pre-equilibrium qcd dynamics? *The European Physical Journal C*, 75(7):305, 2015.
- [44] T. Roser. Rhic performance. *Nuclear Physics A*, 698(1):23 – 28, 2002.
- [45] Björn Schenke, Prithwish Tribedy, and Raju Venugopalan. Fluctuating glasma initial conditions and flow in heavy ion collisions. *Phys. Rev. Lett.*, 108:252301, Jun 2012.
- [46] Bjrn Schenke and Raju Venugopalan. Collective effects in lightheavy ion collisions. *Nuclear Physics A*, 931:1039 – 1044, 2014. {QUARK} {MATTER} 2014XXIV {INTERNATIONAL} {CONFERENCE} {ON} {ULTRARELATIVISTIC} NUCLEUS-NUCLEUS {COLLISIONS}.

- [47] Sren Schlichting and Bjrn Schenke. The shape of the proton at high energies. *Physics Letters B*, 739:313 – 319, 2014.
- [48] Huichao Song. Hydrodynamic modelling for relativistic heavy-ion collisions at rhic and lhc. *Pramana*, 84(5):703–715, 2015.
- [49] Wilke van der Schee, Paul Romatschke, and Scott Pratt. Fully dynamical simulation of central nuclear collisions. *Phys. Rev. Lett.*, 111:222302, Nov 2013.
- [50] S. Voloshin and Y. Zhang. Flow study in relativistic nuclear collisions by fourier expansion of azimuthal particle distributions. *Zeitschrift für Physik C Particles and Fields*, 70(4):665–671, 1996.
- [51] Kevin Welsh, Jordan Singer, and Ulrich Heinz. Initial-state fluctuations in collisions between light and heavy ions. *Phys. Rev. C*, 94:024919, Aug 2016.
- [52] XIAO-MING XU. ORIGIN OF TEMPERATURE OF QUARK-GLUON PLASMA IN HEAVY ION COLLISIONS, pages 203–208. WORLD SCIENTIFIC, 2015.